Supporting Information for

Synergy of strong/weak interface adhesion forces and Li_2S additive enabling high performance full anode-free lithium-metal batteries

Zejian Fang[ab], Shukai Ding*[a], Gaohui Du*[a], Yong Zhu[c], Christophe A. Serra[d], Bingshe Xu[a], Qingmei Su[a], Guoquan Suo*[b], Wei Wang*[c]

[1] Materials Institute of Atomic and Molecular Science, Shaanxi University of Science and Technology, Xi'an 710021, China

[2] School of Materials Science & Engineering, Shaanxi University of Science and Technology, Xi'an 710021, China.

[3] School of Metallurgical and Ecological Engineering, University of Science and Technology Beijing, Beijing 100083, China

[4] Université de Strasbourg, CNRS, ICS UPR 22, F-67000 Strasbourg, France

***Corresponding author:**

Shukai Ding, E-mail: dingshukai@sust.edu.cn

Gaohui Du, E-mail: dugaohui@sust.edu.cn

Guoquan Suo, E-mail:suoguoquan@sust.edu.cn

Wei Wang, E-mail: wwang@ustb.edu.cn

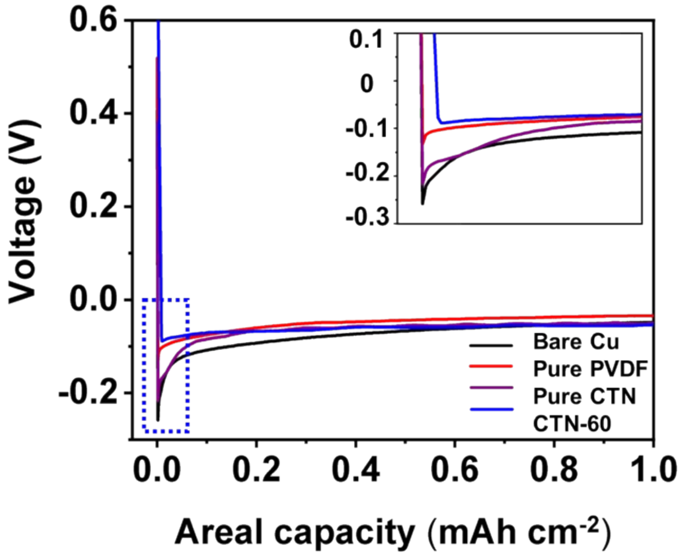

Figure S1 Initial voltage versus areal capacity profiles in half-cell of bare Cu, pure PVDF, pure CTN, and CTN-60 at the current density of 0.5 mA cm^{-2}.

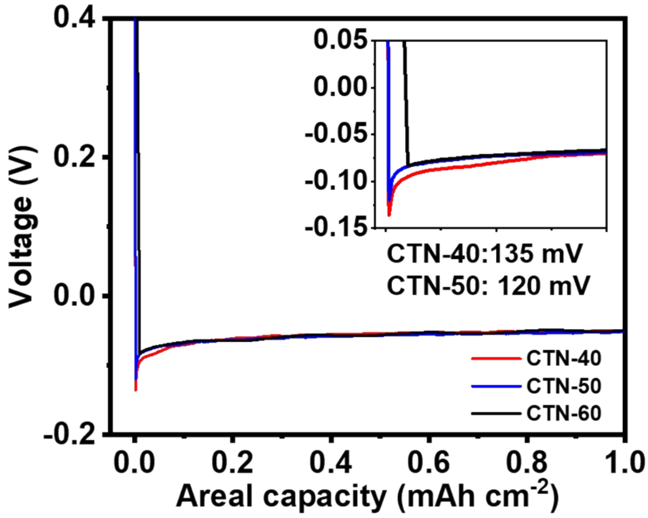

Figure S2 Initial voltage versus areal capacity profiles in half-cell of CTN-40, CTN-50, and CTN-60 at the current density of 0.5 mA cm^{-2}.

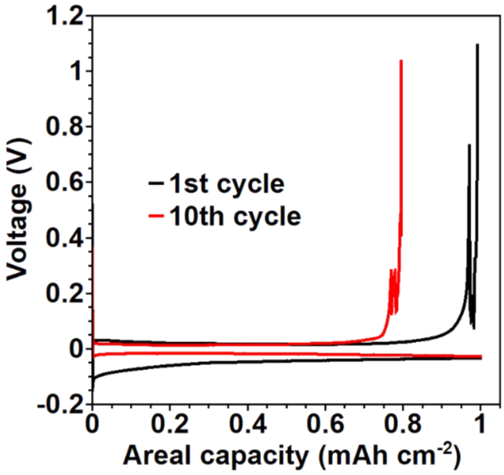

Figure S3 Voltage profiles in the half cell of pure PVDF.

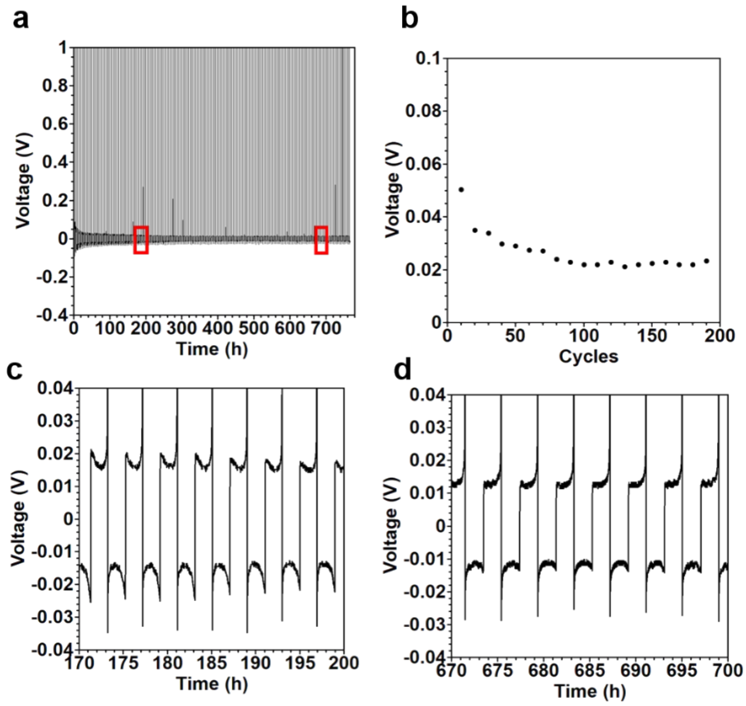

Figure S4 (a) Voltage versus cycle number curve of CTN-60 at 0.5 mA cm^{-2} with an areal capacity of 1 mAh cm^{-2}, (b) voltage hysteresis versus cycle number, and (c, d) voltage profiles of selected cycles.

Table S1 Performance comparison of half-cell in literatures.

Current density (mA cm^{-2})	Capacity (mAh cm^{-2})	Cycles	Average coulombic efficiency (%)	Reference
0.5	1	200	96.08	This work
5	0.5	30	98.83	1
1	0.5	200	98	2
5	0.5	100	90.2	3
1	1	200	97.7	4
1	1	130	97.3	5
0.2	1.5	40	98.1	6
1	1	100	/	7
0.5	1	200	94.5	8
1	0.5	240	97.6	9
0.5	1	150	87	10
1	1	180	97	11
0.25	0.5	300	98.5	12

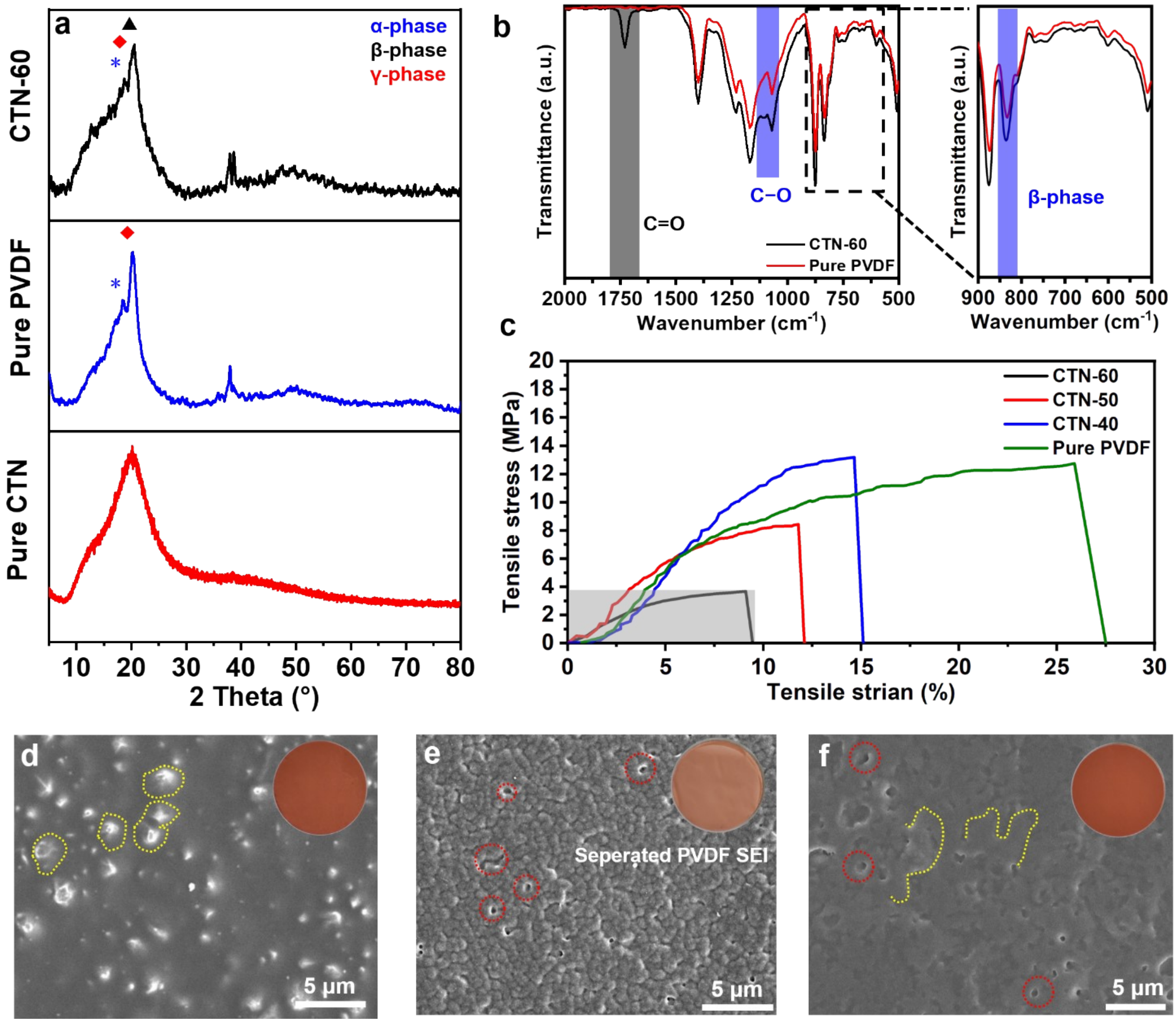

Figure S5 (a) XRD pattern for CTN-60, pure PVDF, and pure CTN, (b) FTIR spectra of pure PVDF and CTN-60, (c) mechanical property of CTN-60, -50, -40, and pure PVDF, morphology (inset: photographs) of (d) pure CTN, (e) pure PVDF, (f) CTN-60 charactered by SEM (yellow dotted line representing the convex formed by aggregation of CTN or crystallizing of PVDF molecule, red dotted circles representing the crack induced by phase segregation).

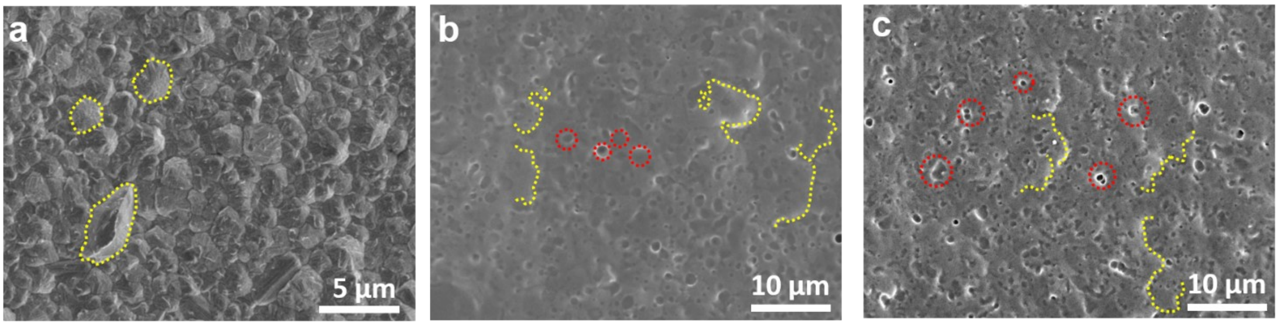

Figure S6 Morphology of (a) bare Cu, (b) CTN-50, and (c) CTN-40 characterized by SEM. (yellow dotted line representing the Cu convex in Figure a and imprinted Cu convex by SEI in Figures b and c, red dotted circles representing the crack induced by phase segregation).

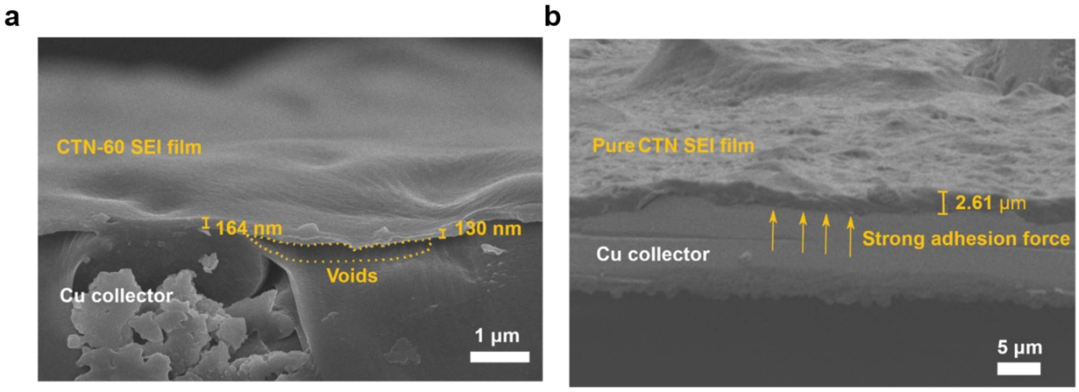

Figure S7 Cross-section of (a) Cu collector with CTN-60 and (b) Cu collector with pure CTN characterized by SEM.

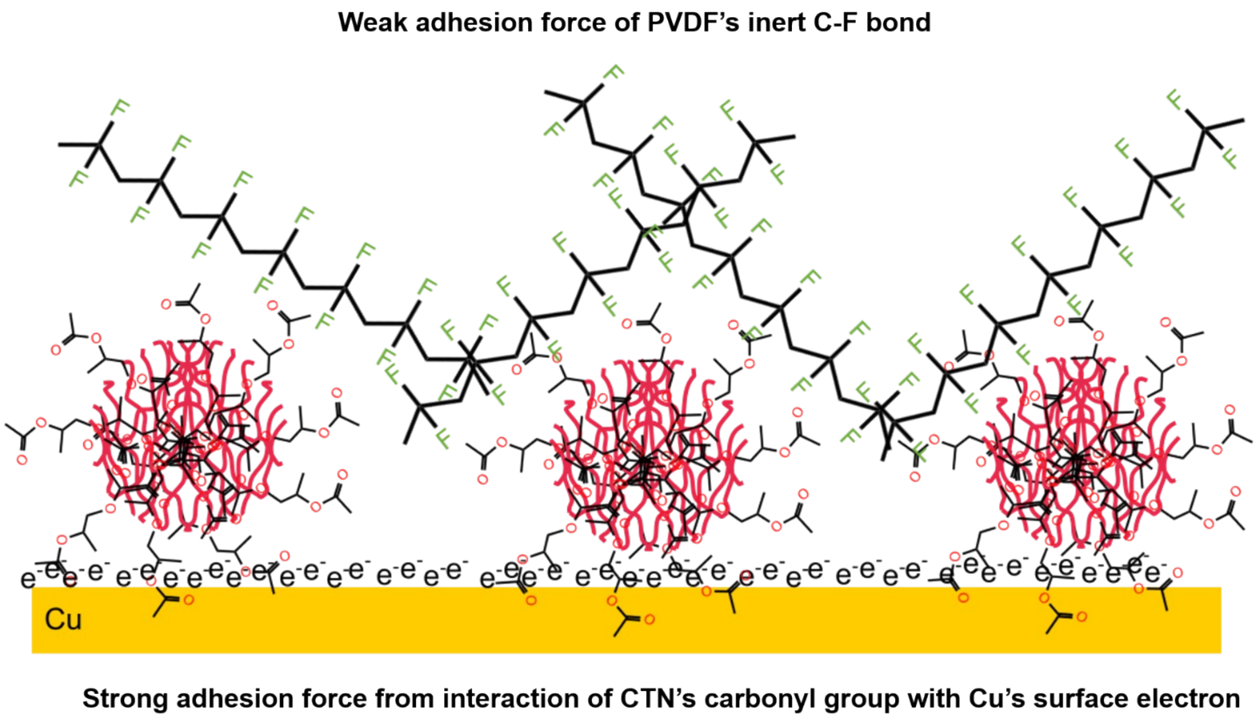

Figure S8 Scheme of the mixed adhesion force of CTN-60 with Cu collector.

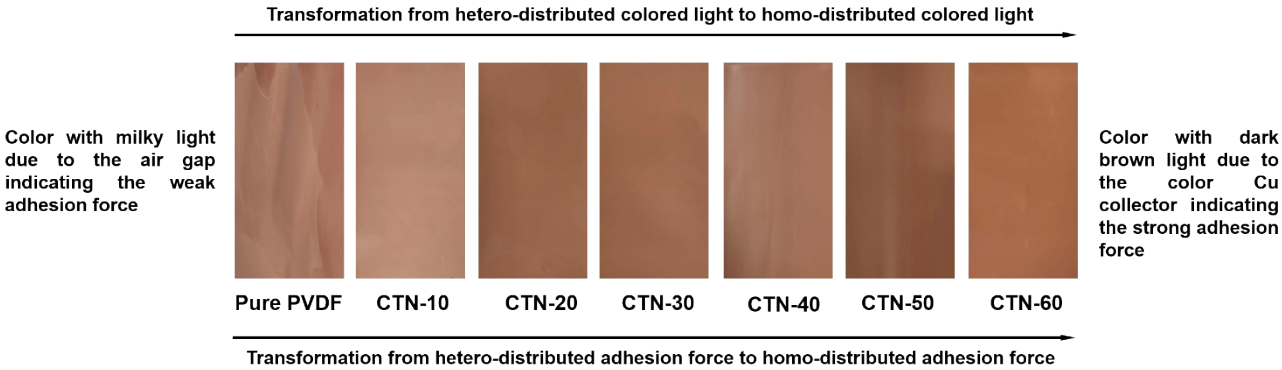

Figure S9 Transformation of visual state characterized by different SEIs photos

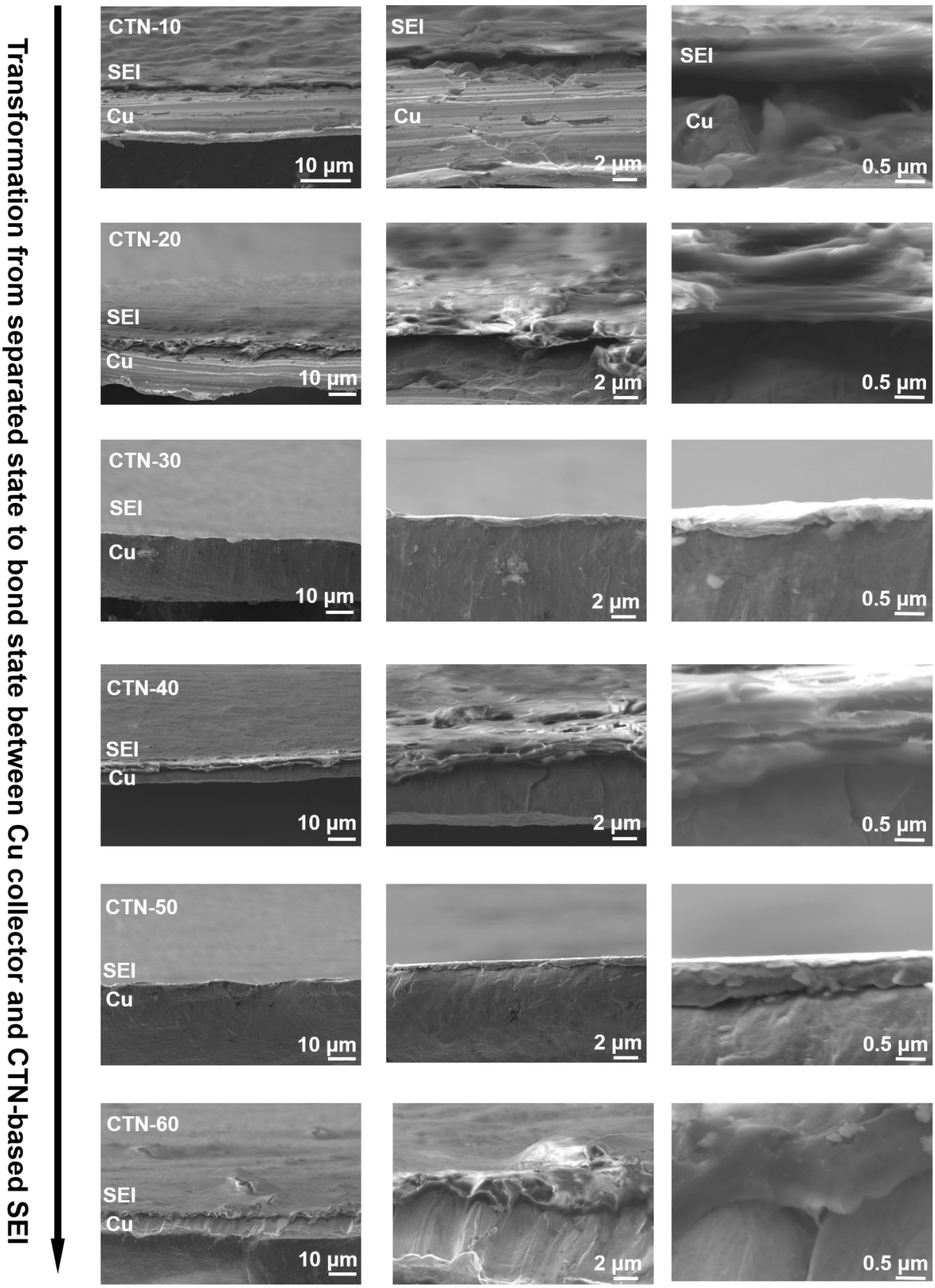

Figure S10 Transformation of different SEIs interfacial state characterized by SEM.

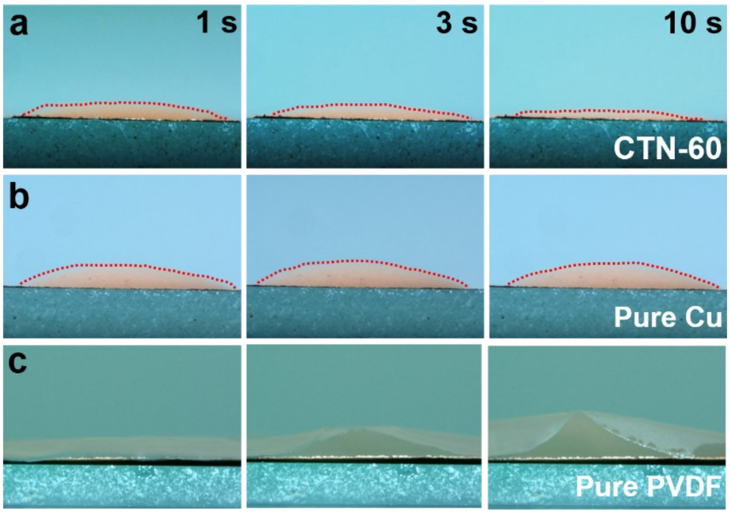

Figure S11 (a) Electrolyte wetting testing of (a) CTN-60, (b) bare Cu, and (c) pure PVDF.

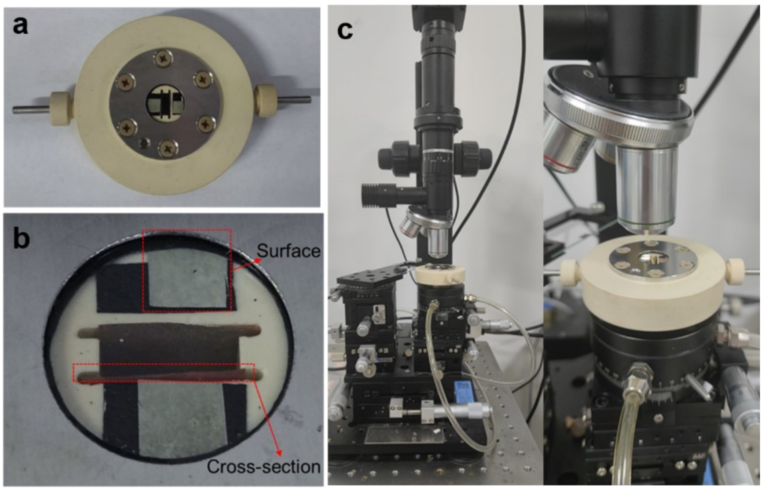

Figure S12 (a) Sealed equipment with glass windows, (b) locations of the sample in sealed equipment for observation the morphology of surface and cross-section, and (c) optical microscope for observation.

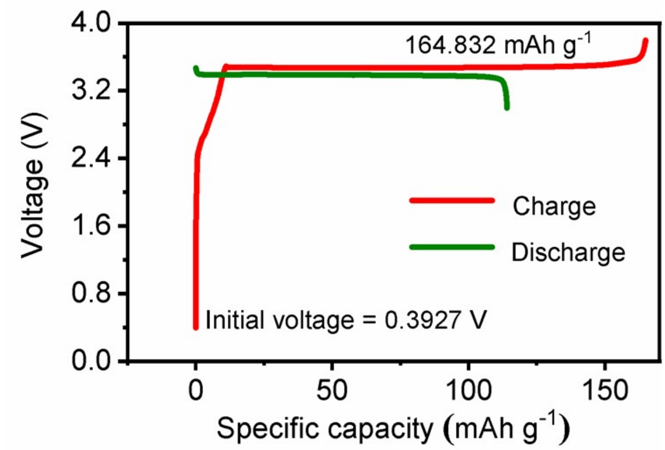

Figure S13 Initial charge and discharge curves of $LiFePO_4$ based full cell with CTN-60.

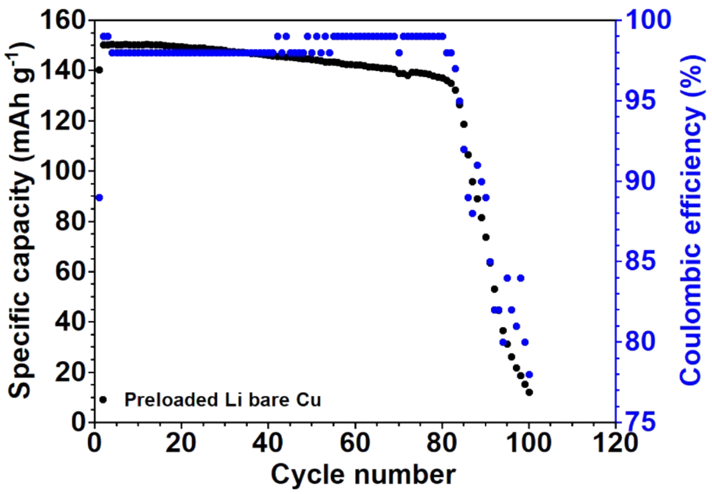

Figure S14 Electrochemical performance of $LiFePO_4$ full cell with the preloaded Li bare Cu with 2 mAh cm^{-2}.

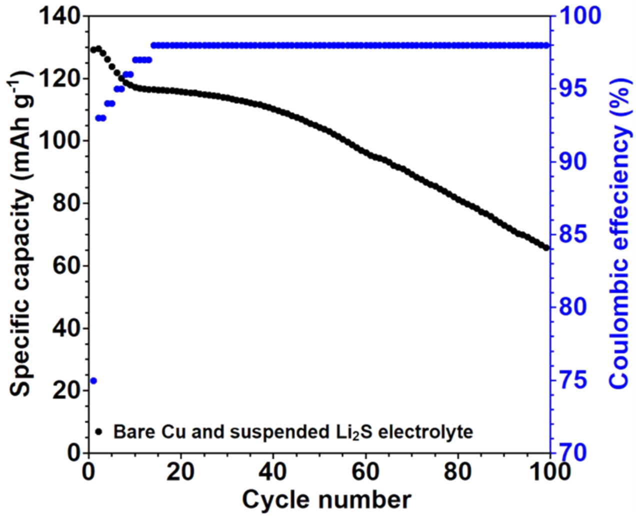

Figure S15 Electrochemical performance of $LiFePO_4$ full cell with the bare Cu and the suspended Li_2S electrolyte.

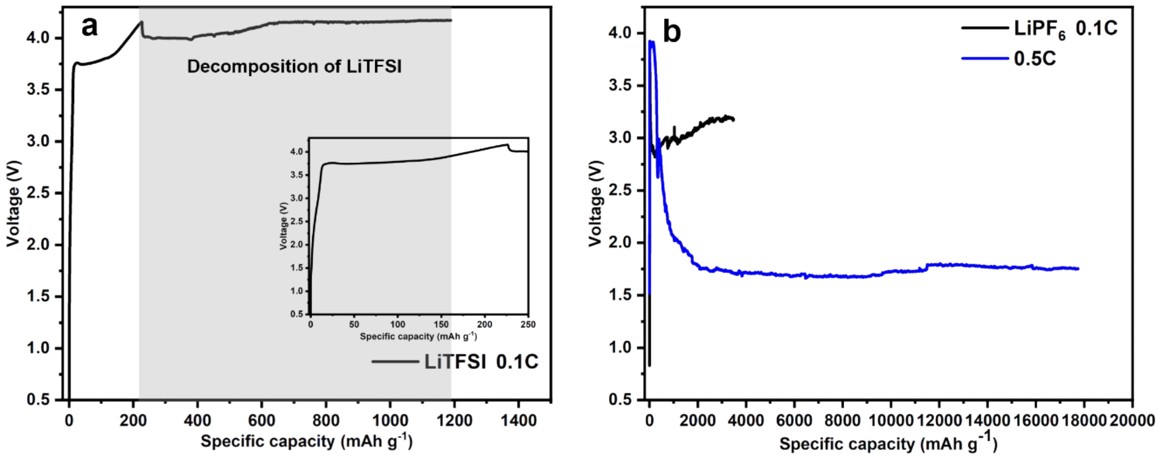

Figure S16 Voltage versus specific capacity curve of NCM 811 full cell with Li_2S (a) 1 M LiTFSI in DOL: DME = 1:1 Vol % with 2 % $LiNO_3$ at current density of 0.1 C and (b) 1M $LiPF_6$ in EC:DEC:EMC=1:1:1 Vol% at current density of 0.1 C and 0.5 C, respectively.

Table S2 Performance comparison of full-cell in literatures.

Collector	Cathode	Electrolyte	Current rate	Cycles	Capacity retention (%)	Ref.
Cu@CTN-60	LFP	1 M LiTFSI + 2%$LiNO_3$ in DOL: DME (1:1, v/v) +2%Li_2S	2C (1.19 mA cm^{-2})	100	85.98%	This work
Cu@LiF-PVDF	LFP	1 M LiTFSI + 2%$LiNO_3$ in DOL: DME (1:1, v/v)	1C	40	~18.5%	3
Cu|Ag@PDA-GO	NCM	1 M $LiPF_6$ in EC/DEC (1:1 v/v) with 5% FEC	0.5 mA cm^{-2}	50	65.47%	6
Cu@MLG	LFP	1 M LiTFSI + 2%$LiNO_3$ in DOL: DME (1:1, v/v)	0.1C	100	60.92%	7
Cu@PEO	LFP	1 M LiTFSI + 2%$LiNO_3$ in DOL: DME (1:1, v/v)	0.2C	100	49.6%	10
Cu	NCM622	2.3 M LiFSI and 4.6 M LiTFSI in DME	C/3	55	~55.62%	13
Cu@GO	NCM	1 M $LiPF_6$ in EC/DEC (1:1 v/v) with 5% FEC	0.2 mA cm^{-2}	20	46.32%	14
3DLN	LFP	1 M $LiPF_6$ in EC/DM (1:1, v/v)	0.5 mA cm^{-2}	100	49.1%	15
Cu	NCM111	2 M $LiPF_6$ in EC/DEC+50% FEC	0.2 mA cm^{-2}	50	40%	16
Cu	LFP	2 M LiFSI + 1 M LiTFSI in DOL/DME (1:1, v/v)	0.2 mA cm^{-2}	100	33.3%	17
Cu	LFP	4 M LiFSI in DME	0.2 mA cm^{-2}	50	52%	18

Reference

(1) Lin, L.; Suo, L.; Hu, Y. sheng; Li, H.; Huang, X.; Chen, L. Epitaxial Induced Plating Current-Collector Lasting Lifespan of Anode-Free Lithium Metal Battery. *Adv. Energy Mater.* **2021**, *11* (9), 1–8. https://doi.org/10.1002/aenm.202003709.

(2) Luo, J.; Fang, C. C.; Wu, N. L. High Polarity Poly(Vinylidene Difluoride) Thin Coating for Dendrite-Free and High-Performance Lithium Metal Anodes. *Adv. Energy Mater.* **2018**, *8* (2), 1–7. https://doi.org/10.1002/aenm.201701482.

(3) Tamwattana, O.; Park, H.; Kim, J.; Hwang, I.; Yoon, G.; Hwang, T. H.; Kang, Y. S.; Park, J.; Meethong, N.; Kang, K. High-Dielectric Polymer Coating for Uniform Lithium Deposition in Anode-Free Lithium Batteries. *ACS Energy Lett.* **2021**, *6* (12), 4416–4425. https://doi.org/10.1021/acsenergylett.1c02224.

(4) Fu, A.; Wang, C.; Peng, J.; Su, M.; Pei, F.; Cui, J.; Fang, X.; Li, J. F.; Zheng, N. Lithiophilic and Antioxidative Copper Current Collectors for Highly Stable Lithium Metal Batteries. *Adv. Funct. Mater.* **2021**, *31* (15), 1–9. https://doi.org/10.1002/adfm.202009805.

(5) Lee, J. H.; Cho, Y. G.; Gu, D.; Kim, S. J. 2D $PdTe_2$Thin-Film-Coated Current Collectors for Long-Cycling Anode-Free Rechargeable Batteries. *ACS Appl. Mater. Interfaces* **2022**, *14* (13), 15080–15089. https://doi.org/10.1021/acsami.1c21183.

(6) Wondimkun, Z. T.; Tegegne, W. A.; Shi-Kai, J.; Huang, C. J.; Sahalie, N. A.; Weret, M. A.; Hsu, J. Y.; Hsieh, P. L.; Huang, Y. S.; Wu, S. H.; Su, W. N.; Hwang, B. J. Highly-Lithiophilic Ag@PDA-GO Film to Suppress Dendrite Formation on Cu Substrate in Anode-Free Lithium Metal Batteries. *Energy Storage Mater.* **2021**, *35*, 334–344. https://doi.org/10.1016/j.ensm.2020.11.023.

(7) Assegie, A. A.; Chung, C. C.; Tsai, M. C.; Su, W. N.; Chen, C. W.; Hwang, B. J. Multilayer-Graphene-Stabilized Lithium Deposition for Anode-Free Lithium-Metal Batteries. *Nanoscale* **2019**, *11* (6), 2710–2720. https://doi.org/10.1039/c8nr06980h.

(8) Zhu, B.; Jin, Y.; Hu, X.; Zheng, Q.; Zhang, S.; Wang, Q.; Zhu, J. Poly(Dimethylsiloxane) Thin Film as a Stable Interfacial Layer for High-Performance Lithium-Metal Battery Anodes. *Adv. Mater.* **2017**, *29* (2), 1–6. https://doi.org/10.1002/adma.201603755.

(9) Liu, W.; Lin, D.; Pei, A.; Cui, Y. Stabilizing Lithium Metal Anodes by Uniform Li-Ion Flux Distribution in Nanochannel Confinement. *J. Am. Chem. Soc.* **2016**, *138* (47), 15443–15450. https://doi.org/10.1021/jacs.6b08730.

(10) Assegie, A. A.; Cheng, J. H.; Kuo, L. M.; Su, W. N.; Hwang, B. J. Polyethylene Oxide Film Coating Enhances Lithium Cycling Efficiency of an Anode-Free Lithium-Metal Battery. *Nanoscale* **2018**, *10* (13), 6125–6138. https://doi.org/10.1039/c7nr09058g.

(11) Zheng, G.; Wang, C.; Pei, A.; Lopez, J.; Shi, F.; Chen, Z.; Sendek, A. D.; Lee, W.; Lu, Z.; Schneider, H.; Safont-sempere, M. M.; Chu, S.; Bao, Z.; Cui, Y. High Performance Lithium Metal Negative Electrode with a Soft and Flowable Polymer Coating. *ACS Energy Lett* **2016**, *1* (6), 1247–1255. https://doi.org/10.1021/acsenergylett.6b00456.

(12) Liu, Y.; Lin, D.; Yuen, P. Y.; Liu, K.; Xie, J.; Dauskardt, R. H.; Cui, Y. An Artificial Solid Electrolyte Interphase with High Li-Ion Conductivity, Mechanical Strength, and Flexibility for Stable Lithium Metal Anodes. *Adv. Mater.* **2017**, *29* (10), 1–8. https://doi.org/10.1002/adma.201605531.

(13) Alvarado, J.; Schroeder, M. A.; Pollard, T. P.; Wang, X.; Lee, J. Z.; Zhang, M.; Wynn, T.; Ding, M.; Borodin, O.; Meng, Y. S.; Xu, K. Bisalt Ether Electrolytes: A Pathway towards Lithium Metal Batteries with Ni-Rich Cathodes. *Energy Environ. Sci.* **2019**, *12* (2), 780–794. https://doi.org/10.1039/c8ee02601g.

(14) Wondimkun, Z. T.; Beyene, T. T.; Weret, M. A.; Sahalie, N. A.; Huang, C. J.; Thirumalraj, B.; Jote, B. A.; Wang,

D.; Su, W. N.; Wang, C. H.; Brunklaus, G.; Winter, M.; Hwang, B. J. Binder-Free Ultra-Thin Graphene Oxide as an Artificial Solid Electrolyte Interphase for Anode-Free Rechargeable Lithium Metal Batteries. *J. Power Sources* **2020**, *450*, 227589. https://doi.org/10.1016/j.jpowsour.2019.227589.

(15) Liu, H.; Yue, X.; Xing, X.; Huang, J.; Petrova, V. Author ' s Accepted Manuscript A Scalable 3D Lithium Metal Anode. *Energy Storage Mater.* **2018**, *16*, 505–511. https://doi.org/10.1016/j.ensm.2018.09.021.

(16) Hagos, T. T.; Thirumalraj, B.; Huang, C.; Hadush, L.; Hagos, T. M.; Berhe, G. B.; Bezabh, K.; Cherng, J.; Chiu, S.; Su, W.; Hwang, B. Locally Concentrated LiPF6 in Carbonate-Based Electrolyte with Fluoroethylene Carbonate as a Diluent for Anode-Free Lithium Metal Battery c Amita. *ACS Appl. Mater. Interfaces* **2019**, *11* (10), 9955–9963. https://doi.org/10.1021/acsami.8b21052.

(17) Beyene, T. T.; Bezabh, H. K.; Weret, M. A.; Hagos, T. M.; Huang, C.; Wang, C.; Su, W.; Dai, H.; Hwang, B. Concentrated Dual-Salt Electrolyte to Stabilize Li Metal and Increase Cycle Life of Anode Free Li-Metal Batteries. *J. Electrochem. Soc.* **2019**, *166* (8), 1501–1509. https://doi.org/10.1149/2.0731908jes.

(18) Rodriguez, R.; Loe, K. E.; Edison, R. A.; Stephens, R. M.; Dolocan, A.; Heller, A.; Mullins, C. B. Effect of the Electrolyte on the Cycling E Ffi Ciency of Lithium-Limited Cells and Their Morphology Studied Through in Situ Optical Imaging. *ACS Appl.Energy Mater.* **2018**, *1* (11), 5830–5835. https://doi.org/10.1021/acsaem.8b01194.